Helsinki University of Technology Publications on Engineering Physics
Teknillisen korkeakoulun teknillisen fysiikan julkaisuja
Espoo 2004 TKK-F-A829

# A HYBRID MODEL OF CARDIAC ELECTRICAL CONDUCTION

**Kim Simelius, Jukka Nenonen, Ville Mäntynen, John C. Clements, and B. Milan Horáček**

TEKNILLINEN KORKEAKOULU
TEKNISKA HÖGSKOLAN
HELSINKI UNIVERSITY OF TECHNOLOGY
TECHNISCHE UNIVERSITÄT HELSINKI
UNIVERSITE DE TECHNOLOGIE D'HELSINKI

Helsinki University of Technology Publications on Engineering Physics
Teknillisen korkeakoulun teknillisen fysiikan julkaisuja
Espoo 2004 TKK-F-A829

# A HYBRID MODEL OF CARDIAC ELECTRICAL CONDUCTION

**Kim Simelius, Jukka Nenonen, Ville Mäntynen, John C. Clements, and B. Milan Horáček**

From the Laboratory of Biomedical Engineering, Helsinki University of Technology,
and BioMag Laboratory, Helsinki University Central Hospital, Helsinki, Finland (KS, JN & VM);
Department of Mathematics & Statistics (JCC), and Department of Physiology & Biophysics (BMH),
Dalhousie University, Halifax, NS, Canada.

TEKNILLINEN KORKEAKOULU
TEKNISKA HÖGSKOLAN
HELSINKI UNIVERSITY OF TECHNOLOGY
TECHNISCHE UNIVERSITÄT HELSINKI
UNIVERSITE DE TECHNOLOGIE D'HELSINKI

Distribution:
Helsinki University of Technology
Department of Engineering Physics and Mathematics
Laboratory of Biomedical Engineering
P.O.Box 2200
FIN-02015 HUT
FINLAND
Tel. +358-9-4513172
Fax. +358-9-4513182

ISBN 951-22-7026-9
ISSN 1459-7268

# ABSTRACT

We describe accurate algorithms for simulating propagated electric activation in three-dimensional anisotropic cardiac muscle, based on bidomain theory under subthreshold conditions and governed by a cellular automaton when an action potential is elicited. In a bidomain formulation, we represent the anisotropic electric properties of cardiac muscle by conductivity tensors $G_i$ and $G_e$ in intracellular and extracellular domains, separated by a cell membrane with capacitance $c_m$ per unit area. For an equal anisotropy ratio ($G_i = kG_e$), propagated activation is described by a parabolic reaction-diffusion equation for the transmembrane potential. For general anisotropies ($G_i \neq kG_e$), the transmembrane and extracellular potentials need to be solved from a coupled system of parabolic and elliptic partial differential equations. We show how this full system can be decoupled into one parabolic system of reaction-diffusion type by introducing the harmonic means of conductivities in the intracellular and extracellular domains. We also describe an algorithm that accounts for a size of model cells which are larger than the thickness of the wave front and thus permit the accurate simulation on a macroscopic scale. We found that the decoupling via the harmonic-mean approximation of bidomain conductivities allows physiologically accurate simulations of cardiac electric propagation phenomena in a manner that is computationally tractable.


**Keywords:** Bidomain model, cellular automata, computer simulation, cardiac electric activation.


# INTRODUCTION

Following classical papers of Wiener and Rosenblueth [50] and Moe and co-workers [27], early models of electric propagation phenomena in the heart used automata with a small number of discrete states to simulate electrophysiologic behavior of cardiac muscle (see review [12]). Emergence of bidomain theory for the macroscopic description of cardiac electric properties [11, 34, 41, 48] opened the door to physiologically accurate simulations of cardiac propagation phenomena, and with the advent of high-performance computing in the 1990s, anatomically and physiologically realistic whole-heart models became feasible [1, 4, 20, 36, 54]. However, despite important theoretical and computational advances, numerical simulations of the propagated electric activation in the anatomically and physiologically accurate models of the whole heart still pose a formidable computational challenge [3, 14, 35]. In general, the computation time in heart-model simulations depends on the spatial resolution, being approximately proportional to the fourth power of the cell-array dimensions. The state-of-the-art *macroscopic* description of cardiac muscle involves a bidomain model with unequal anisotropy ratios in intracellular and extracellular space [13]; this entails solution of coupled systems of partial differential equations, resulting in a very large sparse-matrix problem [14]. Such bidomain simulations—especially when a detailed description of transmembrane ionic currents is included—require high-performance computing facilities, even for simple parallelepiped slab geometries [3].

Accordingly, in an attempt to keep the whole-heart simulations tractable, we have adopted a hybrid approach introduced by Leon and Horáček [23], which has been previously used in blocks of cardiac muscle [17, 23], an ellipsoidal left ventricle [24, 25], and in an anatomically realistic structure representing human ventricular myocardium [18, 19, 31]. Computation of the propagated excitation proceeds rapidly in this model, and captures the essential behavior of advancing wave fronts in the ventricular myocardium with complex rotational anisotropy. The objective of the present paper is to show how to account for the unequal anisotropy ratios in cardiac muscle and how to correct for the effects that arise when the size of the model cells are large in relation to actual cardiomyocytes. Using simulations in a parallelepiped slab geometry, we show how the simplifying assumptions regarding anisotropic bidomain conductivities and the size of model cells affect the propagation of electric excitation.

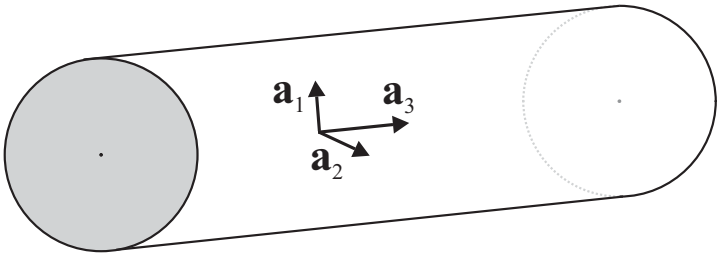


Figure 1: A schematic presentation of a cardiac cell with cylindrical symmetry. The axis $\mathbf{a}_3$ is parallel with longitudinal fiber direction and the axes $\mathbf{a}_1$ and $\mathbf{a}_2$ are in the transverse plane perpendicular to fiber direction.

# THEORY

## Basic concept of the hybrid model

Leon and Horáček introduced a hybrid model of cardiac muscle [23], with features that combine properties of continuous and automata models [35]. Their model overcomes the limitations of abrupt state transitions in automata by permitting subtle summation of electrotonic currents in the anisotropic bidomain under subthreshold conditions and by incorporating precomputed realistic action potentials (APs) under trans-threshold conditions. Algorithms of the hybrid model were described in detail by Nenonen *et al.* [30], and their brief description appears below under Computational Methods.

## Macroscopic continuum model of cardiac muscle

The bidomain theory for macroscopic description of the electric properties of the myocardium rests on the assumption that the cardiac muscle functions as an electrically conductive syncytium consisting of two interpenetrating domains, one intracellular ($i$) and one extracellular/interstitial ($e$), separated by the semi-permeable cell membrane with capacitance $c_m$ per unit area [13]. Cardiac muscle is represented as the anisotropic bidomain region $H$, which consists of a system of cylindrical myocardial fibers with anisotropic electric conductivity [7]; $H$ is embedded in a bounded, insulated and isotropic conducting medium $B$ (body or tissue bath). The fibers are thought to be organized on sheet structures which are layered between the endo- and epicardial surfaces and together constitute the complex three-dimensional myocardial fiber architecture [46]. A tissue structure in $H$ is assumed to have *longitudinal* fiber direction defined by a unit vector $\mathbf{a}_\ell(\mathbf{x})$, that is allowed to vary with position $\mathbf{x}$, and a *transverse* unit vector $\mathbf{a}_t(\mathbf{x})$ that is perpendicular to $\mathbf{a}_\ell(\mathbf{x})$. Intracellular and interstitial domains share the same vectors $\mathbf{a}_\ell(\mathbf{x})$ and $\mathbf{a}_t(\mathbf{x})$. The local basis consisting of an orthogonal set (Fig. 1) is chosen at $\mathbf{x}$ so that a unit vector $\mathbf{a}_3(\mathbf{x})$ is parallel with $\mathbf{a}_\ell(\mathbf{x})$ and unit vectors $\mathbf{a}_1(\mathbf{x})$ and $\mathbf{a}_2(\mathbf{x})$ (and all vectors coplanar with them) are said to be in the transverse direction at $\mathbf{x}$. In the local basis, the intracellular conductivities along the axes are $\sigma_t^i, \sigma_t^i, \sigma_\ell^i$, and the corresponding interstitial conductivities are $\sigma_t^e$, $\sigma_t^e$, and $\sigma_\ell^e$. When uniform anisotropy is assumed, the scalar constants $\sigma_t^{i,e}$ and $\sigma_\ell^{i,e}$ are independent of $\mathbf{x}$.

## Accurate representation of anatomical anisotropy

For anatomically accurate whole-heart modeling, it is necessary to incorporate the counterclockwise rotation of fibers within the ventricular wall, which is the determinant of electric anisotropy; moreover, evaluation of longitudinal and transverse electrotonic currents in an anisotropic bidomain requires that second-rank tensors $G_i$ and $G_e$ be used to describe adequately the intracellular and interstitial anisotropic conductivities [7, 40]. When the local basis is set as in Fig. 1, these tensors are diagonal, $G_{i,e}^* = \mathrm{diag}(\sigma_1^{i,e}, \sigma_2^{i,e}, \sigma_3^{i,e})$. Variable fiber direction in the ventricular myocardium can be described in the

global Cartesian coordinate system (e.g., we use one with $z$ axis pointing from the left-ventricular apex to the root of the aorta), in which the local basis is defined at any $\mathbf{x}$ as $A = (\mathbf{a}_t(\mathbf{x}), \mathbf{a}_t(\mathbf{x}), \mathbf{a}_\ell(\mathbf{x}))$. Tensors $G_i^*$ and $G_e^*$ can be transformed into the global system by rotating the local basis. This is accomplished by multiplying them on each side by a rotation matrix $A$: $G_{i,e} = AG_{i,e}^*A^T$, where the superscript $T$ denotes matrix transpose. Thus, in the global coordinate system the conductivity tensors become [7]

$$G_{i,e} = (\sigma_\ell^{i,e} - \sigma_t^{i,e})\mathbf{a}_\ell\mathbf{a}_\ell^T + \sigma_t^{i,e}I, \tag{1}$$

where $I$ is the identity matrix. Since $\sigma_\ell^{i,e} > \sigma_t^{i,e}$, according to Eq. 1 an anisotropic medium can be thought of as having isotropic conductivities $\sigma_t^{i,e}$ throughout, plus the conductivity "boost" $(\sigma_\ell^{i,e} - \sigma_t^{i,e})$ along the fiber direction.

In addition to conductivity tensors $G_i$ and $G_e$, we will use a conductivity tensor $G_b = G_i + G_e$ for the composite medium of the *bulk* cardiac muscle, a conductivity tensor $G' = kG_i/(k+1) = G_e/(k+1)$ in the bidomain under condition of *equal anisotropy ratio* ($G_e = kG_i$) [34], and a conductivity tensor with harmonic mean values $\sigma''_{\ell,t} = \sigma^i_{\ell,t}\sigma^e_{\ell,t}/(\sigma^i_{\ell,t} + \sigma^e_{\ell,t})$

$$G'' = A\ \mathrm{diag}\left(\sigma''_t, \sigma''_t, \sigma''_\ell\right) A^T \tag{2}$$

in the bidomain under condition of *unequal anisotropy ratio* ($G_e \neq kG_i$) [5].

## Electric potential distribution and current flow

Electric potential and current density are defined in $H$ as macroscopic quantities, which may be considered to be averages over small volumes which are, nevertheless, still encompassing many cardiomyocytes. The intracellular and interstitial current densities are defined as $\mathbf{J}_i = -G_i\nabla\phi_i$ and $\mathbf{J}_e = -G_e\nabla\phi_e$ in $H$, respectively. Here $\phi_i$ and $\phi_e$ are the electric potentials in the intracellular and interstitial domains. The transmembrane potential is defined in $H$ as $v_m = \phi_i - \phi_e$. The total macroscopic current density is [11] $\mathbf{J} = \mathbf{J}_i + \mathbf{J}_e = -G_i\nabla\phi_i - G_e\nabla\phi_e$.

The associated volume-conductor problem can be treated as a quasi-static one [33]. Under this assumption, the conservation law requires that $\nabla \cdot \mathbf{J} = 0$. Then it can be shown that [11]

$$\mathbf{J} = -G_i\nabla v_m - G_b\nabla\phi_e\ . \tag{3}$$

The first term in Eq. 3 is driven by the electrochemical generators in the cardiomyocytes, while the second term represents passive return currents in the tissue. Conservation of $\mathbf{J}$ leads directly to a partial differential equation in $\phi_e$, with a source term that involves the gradient of the transmembrane potential $v_m$

$$\nabla \cdot G_b\nabla\phi_e = -\nabla \cdot G_i\nabla v_m\ . \tag{4}$$

Thus, the distribution of the interstitial potential, $\phi_e$, is related by Eq. 4 to the current sources. Equation 4 suggests that $H$ can be regarded as a composite medium characterized by the bulk conductivity tensor $G_b$, in which there is a distributed impressed current density (a current dipole moment per unit volume), defined by the term $\mathbf{J}^i = -G_i\nabla v_m$ [33].

From cable theory [21], we can obtain another partial differential equation that relates the spatial distribution of interstitial potential and the membrane dynamics [7]:

$$c_m\frac{\partial v_m}{\partial t} + i_{\mathrm{ion}}(v_m) - i_{\mathrm{app}} = -\nabla \cdot G_e\nabla\phi_e \quad \text{in } H\ . \tag{5}$$

Here $c_m = \chi C_m$, $i_{ion} = \chi I_{ion}$, $i_{app} = \chi I_{app}$, where $\chi$ is the membrane surface area per unit volume of the tissue (surface-to-volume ratio), $C_m$ is the membrane capacitance per unit area of the membrane surface, $I_{ion}$ is the ionic current per unit area of the membrane surface, and $I_{app}$ represents an applied current stimulus to start the activation. (To make the equations more transparent, we will hereafter drop

the applied-current term.) Thus we have in $H$ a system consisting of a nonlinear parabolic equation (Eq. 5) in $v_m$, coupled with an elliptic equation (Eq. 4) in $\phi_e$. In extracardiac region $B$ the electric potential $\phi_o$ obeys the Laplace equation.

The systems in $H$ and $B$ are connected by the boundary conditions at the interface. Let the closed surface $S_H$ be a boundary separating bidomain region $H$ and surrounding volume conductor $B$, and let the closed surface $S_B$ bound region $B$; $\mathbf{n}$ will denote the unit outward normal to $S_H$ and $S_B$. Since the potential must be continuous at each boundary and the normal component of current must be continuous across each boundary,

$$\phi_o = \phi_e, \quad \mathbf{n} \cdot \sigma_o \nabla \phi_o = \mathbf{n} \cdot (G_b \nabla \phi_e + G_i \nabla v_m) \quad \text{on } S_H \tag{6}$$

$$\mathbf{n} \cdot \sigma_o \nabla \phi_o = 0 \quad \text{on } S_B. \tag{7}$$

Here $\sigma_o$ is the scalar conductivity in $B$. The bidomain system in $H$ and the passive volume conductor $B$ are connected via the transmission conditions on the boundary $S_H$ (Eq. 6). Since the sources in $H$ are related to the presence of the intracellular medium, which is absent in $B$, we may further assume that $\mathbf{n} \cdot G_i \nabla v_m = 0$ on $S_H$ [7].

Under the condition of equal anisotropy ratio [34]—which requires that $G_e = kG_i$, where $k$ is a scalar constant—Eq. 5 yields the cable equation of electrophysiology [23] in the same form as in the *monodomain* approximation (with grounded interstitial domain, i.e., $\phi_e$ = 0 in $H$):

$$c_m \frac{\partial v_m}{\partial t} = \frac{k}{k+1} \nabla \cdot G_i \nabla v_m - i_{\text{ion}}(v_m) \, . \tag{8}$$

Thus, instead of the coupled partial differential equation system, we need only solve Eq. 8; all terms are in units of electric current (charge per time). This equation can be rewritten to show explicitly the rate of change of transmembrane potential (voltage per time):

$$\frac{\partial v_m}{\partial t} = \nabla \cdot D' \nabla v_m - i_{\text{ion}}(v_m)/c_m \, . \tag{9}$$

The first contribution to $\partial v_m / \partial t$ comes from nearby cells and it is determined from the Laplacian of the transmembrane potential calculated in the local basis of the electrotonic diffusion tensor (in units of area per time), $D' = kG_i/(k+1)c_m$ [52, 53]. The second contribution is due to local transmembrane ionic currents.

Although the monodomain approximation is deemed to be adequate for simulating mere propagation (in contrast to extracellular electrical stimulation), for some applications, Eq. 9 might be an oversimplification. Real cardiac tissue has two distinguishable domains with different anisotropy ratios (with the intracellular conductivity ratio 3- to 6-fold greater than the interstitial one [40]). Thus, we need to consider the bidomain model which incorporates the distinctness of intracellular and extracellular domains [28, 29, 39]. Recently, Clements *et al.* [5] proposed a way to decouple the parabolic equation, Eq. 5, and the elliptic equation, Eq. 4, into a single equation without sacrificing the realistic conductivity characteristics of the bidomain:

$$\begin{aligned} c_m \frac{\partial v_m}{\partial t} - \nabla \cdot G'' \nabla v_m &= -i_{ion}(v_m) \quad + \\ \epsilon \{ \nabla \cdot (A \, \text{diag}(\sigma_\ell^i + \sigma_\ell^e, 0, 0) A^T) \nabla \phi_e \quad &+ \quad \nabla \cdot (A \, \text{diag}(\sigma_\ell^i, 0, 0) A^T) \nabla v_m \} \, , \end{aligned} \tag{10}$$

where $G''$ is the harmonic mean conductivity tensor given in Eq. 2. The dimensionless decoupling factor $\epsilon$ is given by

$$\epsilon = \frac{\sigma_\ell^i \sigma_t^e - \sigma_t^i \sigma_\ell^e}{(\sigma_\ell^i + \sigma_\ell^e)(\sigma_t^i + \sigma_t^e)} \, , \tag{11}$$

and satisfies $\epsilon < 1$ for all possible values of the parameters $\sigma_{\ell,t}^{i,e}$ (Fig. 2). For weak coupling, Eq. 10 reduces to

$$\frac{\partial v_m}{\partial t} = \nabla \cdot D'' \nabla v_m - i_{\text{ion}}(v_m)/c_m \, , \tag{12}$$

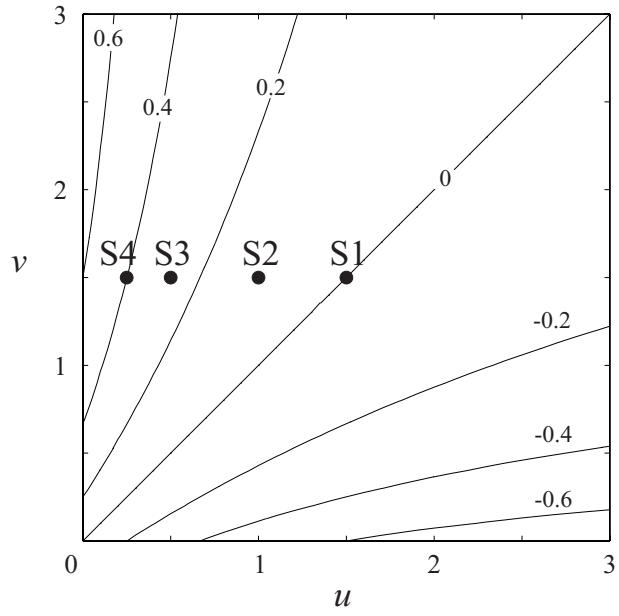


Figure 2: The decoupling factor. The factor $\epsilon$ according to Eq. 11 is represented as isocontour lines in terms of $v = \sigma_t^i/\sigma_t^e$ and $u = \sigma_\ell^i/\sigma_\ell^e$. The dots (S1–S4) refer to the parameter values of the simulations described in Fig. 5.

where the electrotonic diffusion tensor is defined from the Eq. 2 as $D' = G''/c_m$. This approximation is expected to produce nearly the same propagation for $v_m$ as the coupled system of Eqs. 4 and 5, without a need to solve the large sparse system for $\phi_e$ at every time step.

# COMPUTATIONAL METHODS

## Algorithms of the hybrid model

The hybrid model was described in detail in Nenonen *et al.* [30]. Briefly, it is defined as a cellular automaton [2, 47] consisting of $n$ interconnected "cells" (cubes with side $h$), each of which is characterized by a type (e.g., Purkinje, endocardial, epicardial, M-cell) and a fiber direction. The time domain is also discretized, and at each time instant each cell takes on an integer value that defines its *state*. The cell can assume one of the four possible *macrostates*. There are 16 possible macrostate transitions (including identity transformations) among four macrostates, but physiological constraints reduce these transitions to 11. The model obeys a continuous reaction-diffusion partial differential equation for cells in *excitatory* state (below a threshold potential). As soon as the cell reaches a threshold potential, its behavior is ruled by an automaton; initially, the cell switches to its *depolarizing* state, with an upstroke velocity of the AP determined from the cell's previous history and adjusted by using a directional bulk factor (described further below); when the cell reaches a peak transmembrane potential, the automaton sets a predetermined interval for an AP duration with a predefined function representing an AP shape and the cell passes through *refractory* states. As it repolarizes below the threshold potential, it reverts to its *excitatory* state and the reaction-diffusion equation rules again. To reduce computational time early in the simulation, the *quiescent* state is initially assigned to all cells, until they are stimulated externally or until they receive electrotonic current from neighboring cells; under such conditions the cell's state switches from *quiescent* to *excitatory*.

The basic algorithm of a hybrid automaton, simplified from the original description by Nenonen *et al.* [30], is outlined in Table 1. There are only three state variables in the basic hybrid model: $V(i, j, k)$,

**TABLE 1. Algorithm of Hybrid Automaton Model**

| | |
|---|---|
| For each time $t = t + dt$: | |
| For each cell$(i, j, k)$ | |
| (1) Choose new state: | |
| If ($nstat = 1$ and $V^* > 0$) | $nstat = 2$ |
| If ($nstat = 2$ and $V > V_{\rm th}$) | $nstat = 3$; $nclock = {\rm APD}/dt$ |
| If ($nstat = 3$ and $V > V_{\rm max}$) | $nstat = 4$; $V = V_{\rm max}$ |
| If ($nstat = 4$ and $nclock = 0$) | $nstat = 2$; $nclock = 0$; $V = V_{\rm rest}$ |
| (2) Calculate electrotonic current: | |
| Evaluate $V_{\rm xx}$, $V_{\rm yy}$ and $V_{\rm zz}$ for Laplacian | |
| Set stimulus current $I_{app}$ (optional) | |
| $dV/dt = a_{\rm x}V_{\rm xx} + a_{\rm y}V_{\rm yy} + a_{\rm z}V_{\rm zz} + I_{\rm ion} + I_{app}$ | |
| (3) Update cells: | |
| If ($nstat = 1$) | $nclock = nclock + 1$ |
| If ($nstat = 2$) | $V = V + (dV/dt)dt$ (electrotonic); $nclock = nclock + 1$ |
| If ($nstat = 3$) | $V = V + Bdt$ (linear upstroke); $nclock = nclock - 1$ |
| If ($nstat = 4$) | $V = f(nclock, V_{\rm max})$ (AP shape); $nclock = nclock - 1$ |
| Features: | |
| (1) ${\rm APD} = a + (b - a)[1 - exp(-nclock/\tau_1)]$ | transition of state 3 to state 4 |
| (2) $V_{\rm th} = c + d\ exp[-(nclock - ARP)/\tau_2]$ | transition of state 2 to state 3 |
| (3) $V_{\rm max} = h[1 - exp(-nclock/\tau_3)]$ | transition of state 2 to state 3 |
| (4) $I_{\rm ion} = -gV$ (ohmic) | state 2 (subthreshold) |
| (5) $nclock = nclock - pI_{app}$ | state 4 if stimulus on |

$V^*$, transmembrane potential of any of cell's neighbors; $nstat = 1$, *quiescent* state; $nstat = 2$, *excitatory* state; $nstat = 3$, *depolarizing* state; $nstat = 4$, *refractory* state.

$nstat(i, j, k)$, and $nclock(i, j, k)$. As with all models employing synchronous updating, $dV(i, j, k)/dt$ must also be stored for time stepping. Some optional features are added in Table 1 to the basic model to show how its physiological utility can be expanded. Restitution of AP (AP duration as a function of the previous diastolic interval) can be implemented as an exponential function [26], but requires that APD$(i, j, k)$ for all cells be stored. The threshold potential $V_{\rm th}$ and the peak potential $V_{\rm max}$ can be time dependent, in which case $nclock$ mimics recovery of the sodium channel. A background current can be added to electrotonic interactions in the *excitatory* state. External stimulation can force prolongation of the AP by resetting the cell clock back an amount depending on stimulus strength. These added features permit simulations of AP prolongation, decremental conduction, and unidirectional block with an external stimulus or shock.

## Calculation of electrotonic diffusion term

In the cable equation (Eqs. 9 or 12), the rate of change of local transmembrane potential, $\partial v_m/\partial t$, is a sum of contributions from electrotonic interactions generated by the spatial gradient of $v_m$, and from local transmembrane ionic currents. The former contribution is proportional (after appropriate coordinate transformation) to the divergence of the gradient of $v_m$, the Laplacian. In reaction-diffusion systems, the coefficient associated with the Laplacian is called a diffusion coefficient $D$ and it has units of area per time. The electrotonic diffusion *tensor* with dimension of area per time in Eqs. 9 or 12 is the conductivity tensor divided by membrane capacitance per unit area, $D = G/\chi C_m$ [52].

We will demonstrate here in detail how the terms for electrotonic interaction of the form $\nabla \cdot G\nabla\phi$

(where $G = G', G''$) are computed in our discrete model. The purpose of this detailed exposition is to demonstrate the role of the coordinate transformations, which add the extra terms to the Laplacian of the scalar function $\phi$. In global Cartesian coordinates, in which the local basis is specified by azimuth and colatitude angles $\varphi$ and $\theta$, respectively, the conductivity tensor can be written as [17]

$$G = \begin{pmatrix} \sigma_{l-t}\sin^2\theta\cos^2\varphi + \sigma_t & \sigma_{l-t}\sin^2\theta\sin\varphi\cos\varphi & \sigma_{l-t}\sin\theta\cos\theta\cos\varphi \\ \sigma_{l-t}\sin^2\theta\sin\varphi\cos\varphi & \sigma_{l-t}\sin^2\theta\sin^2\varphi + \sigma_t & \sigma_{l-t}\sin\theta\cos\theta\sin\varphi \\ \sigma_{l-t}\sin\theta\cos\theta\cos\varphi & \sigma_{l-t}\sin\theta\cos\theta\sin\varphi & \sigma_{l-t}\cos^2\theta + \sigma_t \end{pmatrix}, \tag{13}$$

where we have used the symbol $\sigma_{l-t} = \sigma_l - \sigma_t$, and assumed a cylindrical symmetry with transverse conductivity $\sigma_t$. In the computation of the electrotonic diffusion term in Eqs. 9 and 12, the first step is to evaluate the total electrotonic current. Matrix $G$ can be written as a sum of the general conductivity matrix and the longitudinal "boost" matrix:

$$\begin{aligned} G\nabla\phi &= \sigma_t \mathbf{I} \begin{pmatrix} \frac{\partial\phi}{\partial x} \\ \frac{\partial\phi}{\partial y} \\ \frac{\partial\phi}{\partial z} \end{pmatrix} + \\ &+ \sigma_{l-t} \begin{pmatrix} \sin^2\theta\cos^2\varphi & \sin^2\theta\sin\varphi\cos\varphi & \sin\theta\cos\theta\cos\varphi \\ \sin^2\theta\sin\varphi\cos\varphi & \sin^2\theta\sin^2\varphi & \sin\theta\cos\theta\sin\varphi \\ \sin\theta\cos\theta\cos\varphi & \sin\theta\cos\theta\sin\varphi & \cos^2\theta \end{pmatrix} \begin{pmatrix} \frac{\partial\phi}{\partial x} \\ \frac{\partial\phi}{\partial y} \\ \frac{\partial\phi}{\partial z} \end{pmatrix}. \end{aligned} \tag{14}$$

The whole electrotonic diffusion term is next evaluated as the divergence of the electrotonic current field (Eq. 15 below) divided by the capacitance per unit area, $c_m$.

$$\begin{aligned} \nabla\cdot G\nabla\phi &= \sigma_t\left(\frac{\partial^2\phi}{\partial x^2} + \frac{\partial^2\phi}{\partial y^2} + \frac{\partial^2\phi}{\partial z^2}\right) \\ &+ \sigma_{l-t}\left(\sin^2\theta\cos^2\varphi\frac{\partial^2\phi}{\partial x^2} + \sin^2\theta\sin^2\varphi\frac{\partial^2\phi}{\partial y^2} + \cos^2\theta\frac{\partial^2\phi}{\partial z^2}\right. \\ &+ 2\sin^2\theta\sin\varphi\cos\varphi\frac{\partial^2\phi}{\partial x\partial y} + 2\sin\theta\cos\theta\cos\varphi\frac{\partial^2\phi}{\partial x\partial z} \\ &+ \left. 2\sin\theta\cos\theta\sin\varphi\frac{\partial^2\phi}{\partial y\partial z}\right). \end{aligned} \tag{15}$$

## Alternative calculation of the divergence of electrotonic currents

The terms of the form $\nabla\cdot G\nabla\phi$ (where $G = G', G''$) can be effectively evaluated by surface integration over an arbitrary small volume, using the Gauss identity

$$\int_v \nabla\cdot G\nabla\phi \;\; dv = \oint_S G\nabla\phi\cdot d\vec{S}. \tag{16}$$

The differential $G\nabla\phi\cdot d\vec{S}$ can be written as

$$\oint_S G\nabla\phi\cdot d\vec{S} = \oint_S \sigma_n\nabla\phi\cdot\vec{u}dS, \tag{17}$$

where $\vec{u}$ is the unit vector from the center of the volume to the surface point, and $\sigma_n$ is the conductivity associated with the direction of the surface normal. The conductivity $\sigma_n$ is given by the expression

$$\sigma_n = \sigma_t + \sigma_{l-t}\left[\begin{pmatrix} \sin^2\theta\cos^2\varphi & \sin^2\theta\sin\varphi\cos\varphi & \sin\theta\cos\theta\cos\varphi \\ \sin^2\theta\sin\varphi\cos\varphi & \sin^2\theta\sin^2\varphi & \sin\theta\cos\theta\sin\varphi \\ \sin\theta\cos\theta\cos\varphi & \sin\theta\cos\theta\sin\varphi & \cos^2\theta \end{pmatrix}\vec{u}\right]\cdot\vec{u}$$

$$
\begin{aligned}
&= \sigma_t + \sigma_{l-t} \begin{pmatrix} \sin^2\theta\cos^2\varphi\ u_x & \sin^2\theta\sin\varphi\cos\varphi\ u_y & \sin\theta\cos\theta\cos\varphi\ u_z \\ \sin^2\theta\sin\varphi\cos\varphi\ u_x & \sin^2\theta\sin^2\varphi\ u_y & \sin\theta\cos\theta\sin\varphi\ u_z \\ \sin\theta\cos\theta\cos\varphi\ u_x & \sin\theta\cos\theta\sin\varphi\ u_y & \cos^2\theta\ u_z \end{pmatrix} \cdot \vec{u} \\
&= \sigma_t + \sigma_{l-t}(\sin^2\theta\cos^2\varphi\ u_x^2 + \sin^2\theta\sin^2\varphi\ u_y^2 + \cos^2\theta\ u_z^2 \\
&\quad +2\sin^2\theta\sin\varphi\cos\varphi\ u_x u_y + 2\sin\theta\cos\theta\cos\varphi\ u_x u_z + 2\sin\theta\cos\theta\sin\varphi\ u_y u_z) \\
&= \sigma_t + \sigma_{l-t}(\sin\theta\cos\varphi\ u_x + \sin\theta\sin\varphi\ u_y + \cos\theta\ u_z)^2 \\
&= \sigma_t + \sigma_{l-t}(\vec{a}\cdot\vec{u})^2, \qquad (18)
\end{aligned}
$$

where $\vec{a}$ is the fiber direction at the center.

### Mean values of variables for macroscopic model cells

When the cable equation (Eqs. 9 or 12) is solved in the discretized model, the relation between the activation wave front thickness and the model's cell-to-cell spacing $h$ has to be considered. A maximum rate of rise of transmembrane potential, $\dot{V}_{\max}$, in human cardiomyocytes [43] is steeper than what a coarse-grained model can simulate (because each model cell typically encompasses hundreds or thousands of cardiomyocytes within its volume $h^3$). Therefore, to represent for computational purposes the *mean* macroscopic values of quantities required for propagating the activation—namely, the slope of the AP upstroke during automaton's suprathreshold *depolarizing* state and the gradient of transmembrane potential during subthreshold *excitatory* state—we have introduced a directional *bulk factor* $B$, which was derived under the following simplifying assumptions.

We assumed that a cubic model cell, occupying a volume $h^3$, is uniformly anisotropic with fiber direction defined by the unit vector $\hat{\mathbf{a}}_\ell$; we further assumed that the propagating activation transits the cell as a plane wave front defined by its unit normal $\hat{\mathbf{n}}$, which makes an angle $\alpha$ with the fiber direction, and it spreads with constant velocity $\vartheta$. Under these assumptions, the bulk factor can be calculated as a ratio of model cells' spacing $h$ and the thickness of the activation wave front, which is estimated from the directional conduction velocity, $\vartheta$, and the direction-dependent risetime of the AP[1] $(V_{\max} - V_{\mathrm{th}})/\dot{V}_{\max}$; thus,

$$
B = \frac{h}{\vartheta(V_{\max} - V_{\mathrm{th}})/\dot{V}_{\max}}. \qquad (19)
$$

Since the activation wave front propagating across model cell only occupies a fraction $1/B$ of the cell's size, the upstroke of the model cell's *mean* AP lasts on average $B$-times longer than the depolarization of one cardiomyocyte from $V_{\mathrm{th}}$ to $V_{\max}$ (because the relatively thin wave front must transit through the relatively thick model cell). Consequently, the rate of depolarization of each model cell during the *depolarizing* state of the automaton must be scaled to $\dot{V}_{\max}/(B+1)$. In the same vein, since the thickness of the wave front propagating across the model cell is a fraction $1/B$ of the cell's size, the computed gradient of transmembrane potential is reduced by a factor of $1/B$ with respect to its true magnitude, and it has to be multiplied by $B$ to obtain a correct mean value over the model cell's volume.

The propagation velocity, $\vartheta$, depends in the anisotropic cardiac muscle on the direction of propagation; in addition, we also assume (departing from the classical bidomain theory) that $\dot{V}_{\max}$ depends on fiber direction. Consequently, we must calculate the bulk factor dynamically, *during* the course of simulation. This is done by calculating first a unit normal to the wave-front surface from the gradient of transmembrane potential and then evaluating the angle $\alpha$ between local longitudinal fiber direction $\hat{\mathbf{a}}_\ell$ and the wave-front's normal $\hat{\mathbf{n}}$ from the dot product $\hat{\mathbf{a}}_\ell \cdot \hat{\mathbf{n}}$. Associated with the longitudinal fiber direction is a nominal value of propagation velocity $\vartheta_\ell$ (Table 2); a propagation velocity in the direction

[1] In continuous bidomain theory [52], it is assumed that the local activation risetime is the same in all directions; however, Spach and Barr [43, 45] have shown that this assumption is not valid due to discontinuous cardiac propagation on microscopic scale. Because the depolarizing phase (AP upstroke) is managed in our hybrid model by a cellular automaton, we can algorithmically adjust directional variables so as to fit the experimentally observed structural complexities of cardiac tissue.

**TABLE 2. Nominal parameters of the hybrid model**

| Parameter | Symbol | Value | Unit | Reference |
|---|---|---|---|---|
| Size of model cells | $h$ | 0.05 | cm | |
| Surface-to-volume ratio* | $\chi$ | 2200 | $\mathrm{cm}^{-1}$ | |
| Specific membrane capacitance | $\mathrm{C_m}$ | 1.0 | $\mu\mathrm{F/cm}^2$ | |
| Maximum $dv_m/dt$ | $\dot{V}_{max,\ell}$ | 120.0 | V/s | [44] |
| | $\dot{V}_{max,t}$ | 160.0 | V/s | [44] |
| Resting potential | $V_{\mathrm{rest}}$ | $-83.0$ | mV | [44] |
| Activation threshold | $V_{\mathrm{th}}$ | $-60.8$ | mV | [37] |
| Longitudinal propagation velocity | $\vartheta_\ell$ | 0.7 | m/s | [37] |
| Simulation time step | $\Delta$t | 10 | $\mu$s | |
| Longitudinal bulk factor** | $\mathrm{B}_\ell$ | 1.07 | – | |
| Transverse bulk factor*** | $\mathrm{B}_t$ | 3.33 | – | |

*$\chi$ corresponds to 100-$\mu$m long cylindrical cells with 10-$\mu$m radius, $\chi = 2(r+l)/rl$
**$B_\ell = (0.05\mathrm{cm} \times 120.0\mathrm{mV/ms})/(0.07\mathrm{cm/ms} \times 80\mathrm{mV}) = 1.07$ (Eq. 19)
***$B_t = (0.05\mathrm{cm} \times 160.0\mathrm{mV/ms})/(0.03\mathrm{cm/ms} \times 80\mathrm{mV}) = 3.33$ (Eq. 19)

transverse to fiber axis, $\vartheta_t$, can be estimated—under the assumptions stated above—as $\vartheta_t = \vartheta_\ell\sqrt{\sigma_t/\sigma_\ell}$. (Note that in the bidomain model, harmonic mean conductivities $\sigma_t''$ and $\sigma_\ell''$ can be used.) Thus, if the activation isochrones are to obey the equation of an ellipse: $(x/\vartheta_\ell)^2 + (y/\vartheta_t)^2 = 1$, where $x = \vartheta\cos\alpha$ and $y = \vartheta\sin\alpha$, the directional conduction velocity should then be

$$\vartheta = \vartheta_\ell/\sqrt{\cos^2\alpha + (\sigma_\ell/\sigma_t)\sin^2\alpha},$$

where $\vartheta_\ell$, $\sigma_t$, and $\sigma_\ell$ are globally defined parameters and the angle $\alpha$ between local fiber direction and local direction of propagation is evaluated during the course of simulation.

The maximum rate of rise of transmembrane potential, $\dot{V}_{\mathrm{max}}$, in our model is dependent on fiber direction according to Spach *et al.* [44]. We recognize $\dot{V}_{max,\ell}$ and $\dot{V}_{max,t}$, associated with longitudinal and transverse propagation, respectively, as nominal parameters globally assigned to the model (Table 2). The $\dot{V}_{\mathrm{max}}$ in the direction that subtends angle $\alpha$ with the local fiber direction is determined analogously with the expression for directional conduction velocity as

$$\dot{V}_{\mathrm{max}} = \dot{V}_{\mathrm{max},\ell}/\sqrt{\cos^2\alpha + (\dot{V}_{\mathrm{max},\ell}/\dot{V}_{\mathrm{max},t})^2\sin^2\alpha}.$$

The directionally-dependent bulk factor, determined during the simulation, is then applied in "packaging" the transmembrane potential, $v_m$, and the transmembrane current, $I_m$. In particular, the rate of rise of the model cell's *mean* AP is calculated from directional $\dot{V}_{\mathrm{max}}$ as $\dot{V}_{\mathrm{max}}/B$, and electrotonic transmembrane currents are computed from the values of transmembrane-potential gradients as $B\nabla v_m$.

## Implementation of the hybrid model

The hybrid model of propagated excitation in the ventricular myocardium has been implemented in Fortran 95 on a four-processor Unix workstation (IBM RS/6000), and in C language on desktop system running Windows NT (SGI Visual PC). For a model with realistic ventricular geometry, we minimized memory usage by allocating space for only those cells that belonged to the myocardial volume. The data of each cell can be accessed by referring to a cubical address volume that has the dimensions of the

model. Furthermore, the addresses of cells in the activation wave front are collected separately into a smaller table to avoid repeatedly going through the whole address cube.

The values we adopted for physiological constants in the bidomain equations are listed in Tables 2 and 3 [6, 40]. Simulations were run in different slabs of tissue with uniform or rotating (from $-45^\circ$ to $45^\circ$) anisotropies. The slab dimensions were 5 cm $\times$ 5 cm $\times$ 2 cm, and the spacing of a regular grid was 0.05 cm.

### Solution of the full system

Besides equal anisotropy ratio, Eq. 9, and the harmonic mean conductivity approximation, Eq. 12, the full system consisting of coupled elliptic and parabolic equations Eqs. 4 and 5 with the appropriate boundary conditions 6 and 7 has been solved to provide a "gold-standard" solution for comparison. Even though the solution is computationally demanding, it can be accomplished by utilizing the sparseness of the discretized problem.

The coupled equation system is solvable also in the context of our hybrid model as follows:

1. Initially, $v_m(t) = v_r$ at $t = 0$ in all cells, and selecting $\phi_i = 0$, $\phi_e(t) = -v_r$ at $t = 0$.
2. When an external stimulus is applied at time $t_k$, solve $v_m(t_{k+1})$ as a function of $\phi_e(t_k)$, applying the explicit forward method to the parabolic Eq. 5.
3. Substitute the resulting $v_m(t_{k+1})$ into the elliptic Eq. 4, and solve for the distribution of $\phi_e(t_{k+1})$.
4. Switch to the next time point and repeat the previous two steps.

In the sparse system solution, we used the PESSL library routine PSPGIS, using an iterative algorithm and a smoothly converging variant of the conjugate gradient squared method (Bi-CGSTAB) as a preconditioner [49]. Iterations were done according to Eq. 15 in Henriquez *et al.* [14].

The Fortran implementation of the full system was ran on an IBM RS/6000 SP high-performance computer at the Scientific Computing Ltd., Espoo, Finland (http://www.csc.fi). In solving the sparse parabolic Eq. 5, we utilized the parallelized ESSL numerical library (http://www.ibm.com/essl.html) and message passing interface (MPI).

## RESULTS

For refinements of the numerical implementation of the hybrid model's propagation algorithm (namely, for testing of the bulk factor and various stencils) we used a slab with uniform anisotropy and dimensions of $50 \times 50 \times 20$ mm ($100 \times 100 \times 40$ cells). We first tested the invariance of the propagation algorithm with respect to the coordinate system. Uniform fiber direction was assigned at three different angles ($0^\circ$, $-45^\circ$, and $65^\circ$) in the planes of $z = \mathrm{const}$. The AP and the transmembrane current were monitored at 5 locations throughout the simulation. Isochrones depicting 25 ms of simulated activation for these three different configurations of the slab are shown in Fig. 3. To assess the shape of the isochrones, an ideal ellipse is plotted along the 25-ms isochrone. The resulting propagation velocity in these simulations was $\vartheta_\ell = 0.7$ m/s in the longitudinal direction of fibers, and $\vartheta_t = 0.3$ m/s in the transverse direction. The propagation ellipsoids obtained without the bulk factor (Eq. 19) exhibited different shapes; due to numerical inaccuracies, the ellipses for $45^\circ$ and $65^\circ$ fiber angles were 'fatter' and those for $0^\circ$ 'slimmer' than the near-ideal ellipses in Fig. 3.

The membrane potential and the transmembrane current from the electrotonic interaction are shown in Fig. 4. The AP foot and upstroke are steeper in the direction of propagation. The transition from bidomain excitation to a cellular automaton at $-60$ mV is not noticeable, and the AP foot follows an

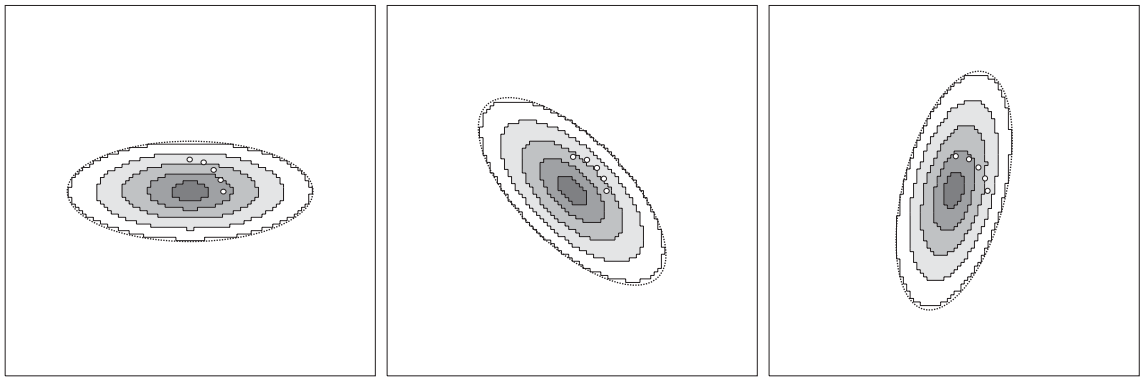

Figure 3: Cross-sectional activation isochrones from simulations in uniformly anisotropic slab with fiber directions of $0°$, $-45°$ and $65°$ in the plane of the cross section. The thicker black line is, in all three images, the same analytically computed ellipse rotated to correspond to the fiber direction. The circles indicate the cells, where the transmembrane AP and the transmembrane current were monitored during simulation. The isochrones are plotted in 5-ms intervals; the slab dimensions are 50 mm or 100 cells in each direction (rectangular outline).

**TABLE 4. Conduction velocities**

| | S1 | S2 | S3 | S4 | Unit |
|---|---|---|---|---|---|
| *Decoupled (Eq. 12)* | | | | | |
| $\vartheta_\ell$ | 0.69 | 0.70 | 0.70 | 0.70 | m/s |
| $\vartheta_t$ | 0.28 | 0.26 | 0.30 | 0.33 | m/s |
| $\vartheta_\ell/\vartheta_t$ | 2.46 | 2.70 | 2.34 | 2.13 | – |
| *Coupled (Eqs. 4 & 5)* | | | | | |
| $\vartheta_\ell$ | 0.69 | 0.73 | 0.79 | 0.86 | m/s |
| $\vartheta_t$ | 0.28 | 0.26 | 0.32 | 0.34 | m/s |
| $\vartheta_\ell/\vartheta_t$ | 2.46 | 2.80 | 2.51 | 2.57 | – |
| Normalized deviation | 1.00 | 1.04 | 1.07 | 1.20 | |

exponential curve (not seen on the plots). In the transmembrane current plots, the ratio of the positive area under the curve to the negative area is approximately 0.7 for all cells.

Next, we rotated the fibers horizontally on each plane to mimic the architecture in the left ventricle. In the bottom ('endocardial') layer the fiber angle was set to $-45°$ (z=0), in the center ('intramural') layer to $0°$ (z=20), and in the top ('epicardial') layer to $+45°$ (z=40). The propagation was simulated both using the full system as described above, and using the decoupled parabolic system of reaction-diffusion type with harmonic means of conductivities in intracellular and extracellular domains (Eq. 12). An initial stimulus was delivered at the center of the 'intramural' layer. The resulting isochrones are shown in Fig. 5.

Propagation velocities were next estimated from these isochrones by fitting an ellipse on the 25-ms isochrone in the intramural layer. The ellipses are sketched on top of the isochrones in Fig. 5. The longitudinal and transversal velocity were evaluated by dividing the distances from the stimulus to the corresponding edge of the ellipse by the time (Table 4).

# DISCUSSION

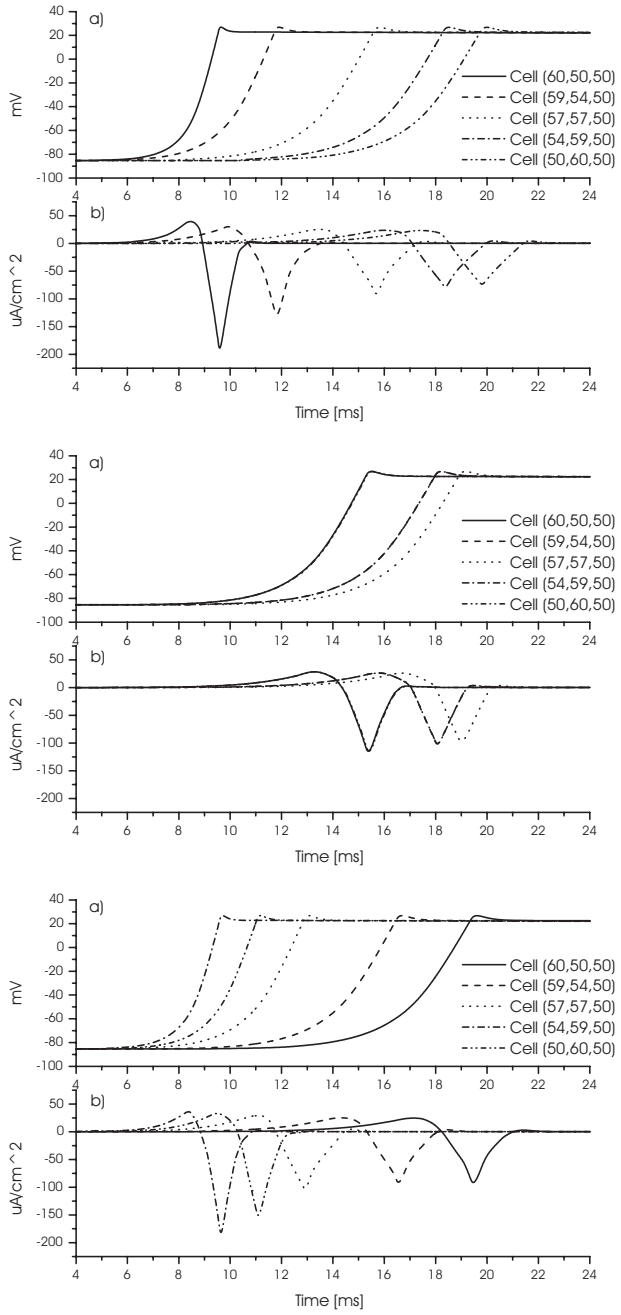


Figure 4: Macroscopic "action potentials" and "transmembrane electrotonic currents" of the cells marked in Fig. 3. The panels (from top to bottom) correspond to fiber directions $0°$, $-45°$ and $65°$, respectively. These AP and $I_m$ functions do *not* represent the recordings that would have been obtained from actual cardiac tissue; rather, they are time-functions of mean quantities $\bar{v}_m$ and $\bar{I}_m$ derived by volume- and time- integration of $v_m$ and $I_m$ over the volume $h^3$ of a given model cell, taking into account variable slope of the AP as a function of direction of propagation, and the variable velocity of propagation in different directions.

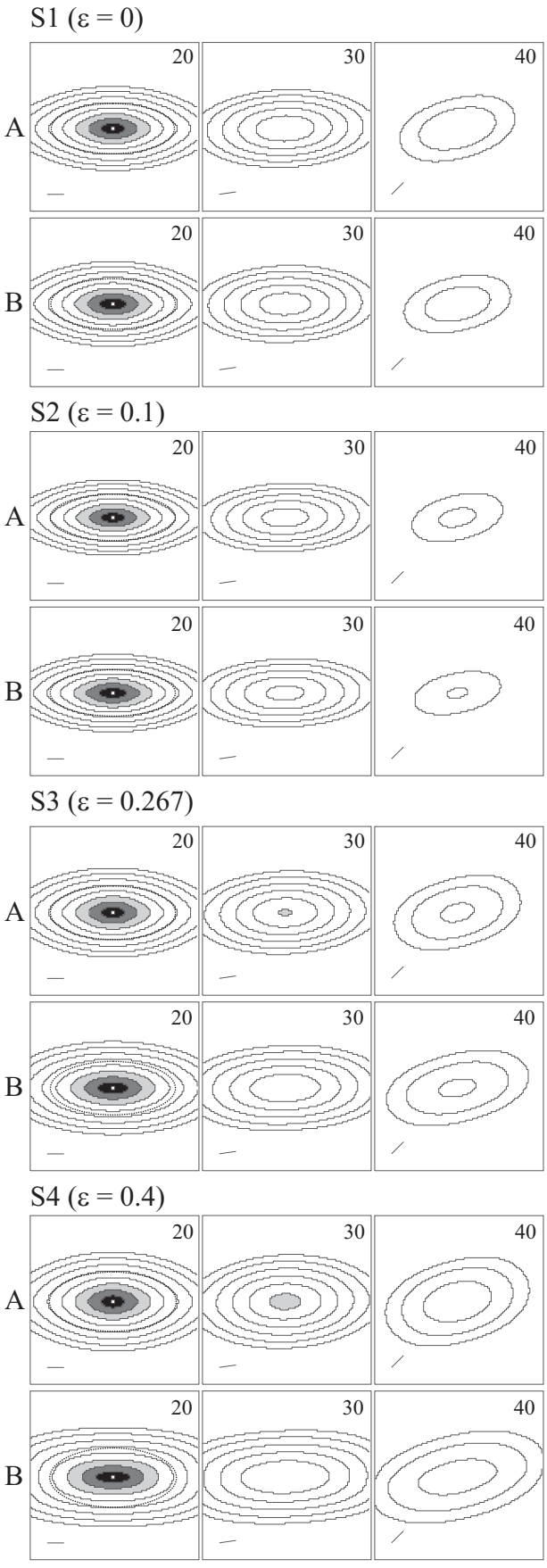


Figure 5: Simulated isochrones for propagated activation in cases S1–S4 marked in Fig. 2. The simulation parameter values are given in Tables 2 and 3. Row A in each case denotes to a decoupled parabolic system of reaction-diffusion type using harmonic mean of conductivities in intracellular and extracellular domains (Eq. 12), while row B refers to a full system with unequal anisotropy ratios, given by coupled parabolic and elliptic equations (Eqs. 4 and 5) with the appropriate boundary conditions (6 and 7).

**TABLE 3. Anisotropic conductivity parameters and directional diffusion coefficients**

| | S1 | S2 | S3 | S4 | Unit |
|---|---|---|---|---|---|
| $\sigma_\ell^i$ | 3.000 | 3.000 | 3.000 | 3.000 | mS/cm |
| $\sigma_t^i$ | 0.495 | 0.330 | 0.330 | 0.330 | mS/cm |
| $\sigma_\ell^e$ | 2.000 | 2.000 | 2.000 | 2.000 | mS/cm |
| $\sigma_t^e$ | 0.330 | 0.330 | 0.660 | 1.320 | mS/cm |
| $\sigma_\ell'' = \frac{\sigma_\ell^i \sigma_\ell^e}{\sigma_\ell^i + \sigma_\ell^e}$ | 1.200 | 1.200 | 1.200 | 1.200 | mS/cm |
| $\sigma_t'' = \frac{\sigma_t^i \sigma_t^e}{\sigma_t^i + \sigma_t^e}$ | 0.198 | 0.165 | 0.220 | 0.264 | mS/cm |
| $\sqrt{\sigma_\ell''/\sigma_t''}$ | 2.462 | 2.697 | 2.335 | 2.132 | – |
| $\epsilon$ | 0.000 | 0.100 | 0.267 | 0.400 | – |
| $D_\ell'' = \sigma_\ell''/c_m$ † | 0.545 | 0.545 | 0.545 | 0.545 | cm$^2$/s |
| $D_t'' = \sigma_t''/c_m$ ‡ | 0.090 | 0.075 | 0.100 | 0.120 | cm$^2$/s |

$\sigma_{\ell,t}''$, harmonic mean conductivities from Eq. 2; $D_{\ell,t}''$, directional diffusion coefficients of the diffusion tensor $D'' = A\ \mathrm{diag}\,(D_t'', D_t'', D_\ell'')\ A^T$.
† $D_\ell''$ should exceed the value of 0.2 cm$^2$/s [52]
‡ $D_t''$ should exceed the value of 0.008 cm$^2$/s [52]

## Diffusion coefficient and its value

Winfree [52, 53] emphasized repeatedly the importance of an electrotonic diffusion coefficient $D$, arguing that everything concerning the spatial pattern of cardiac electric conduction (propagation velocity and its dependence on curvature, liminal length, threshold for stimulation etc.) depends on this quantity with dimension involving space in the cable equation (Eqs. 9 or 12). Based on the assumption that cardiac muscle is an anisotropic *monodomain* represented by longitudinal and transverse intracellular conductivities (with the extracellular space grounded), he identified tentatively a value of the diffusion coefficient as being approximately 1.0 cm$^2$/s and concluded that this value "seems to lie securely within the range required for the assumption of continuous cardiac conduction." In his review/tutorial [52], Winfree focussed on the diffusion coefficient "in its simplest incarnation as a single number (or perhaps three: in longitudinal, transverse, and transmural directions) in monodomain theory, rather than as a tensor in the more refined bidomain model." In the present paper, we use an anisotropic bidomain theory with the assumption of axial symmetry of fibers (thus disregarding possible differences in transverse and transmural conductivities suggested by LeGrice *et al.* [22]), which requires four conductivity parameters (see Table 3). A simple calculation shows that a monodomain estimate of the electrotonic diffusion coefficient $D$ is larger than that based on *bidomain* theory, which is affected by a factor $k/(k+1)$ under the equal anisotropy ratio assumption and by a harmonic mean of conductivities under the unequal anisotropy ratio assumption. Calculation based on the value a longitudinal intracellular conductivity of 2.4 mS/cm (Table 3), surface-to-volume ratio of 2200 cm$^{-1}$, and a specific capacitance of the membrane 1 $\mu$F/cm$^2$ (Table 2) results in a directional electrotonic diffusion coefficient along fibers with a value of 1.09 cm$^2$/s, in agreement with Winfree's estimate. However, since a harmonic-mean conductivity in the longitudinal direction is only 1.2 mS/cm (Table 3), the directional electrotonic diffusion coefficient along fibers in an anisotropic bidomain becomes 0.55 cm$^2$/s, which is not as "securely" within the range required for the assumption of continuous cardiac conduction as the previous Winfree's estimate. This brings us to the fundamental assumption underlying mathematical modelling of cardiac electric conduction.

## Continuous versus discontinuous conduction

Spach [42] reflected recently on the developments of the past 50 years which have advanced our understanding of cardiac electric conduction, and cautioned that a continuous conduction theory of electric propagation phenomena in cardiac muscle does not hold at the microscopic level. This point is well taken. A bidomain theory, assuming that the heart muscle is a syncytial structure, formulates all quantities as macroscopic; that suits perfectly our viewpoint, which *is* macroscopic – aiming at whole-heart simulations taking into account complex three-dimensional anisotropic myocardial fiber architecture. Each "cell" of our hybrid model encompasses, at $h = 0.05$ cm, a very large number ($\sim$3000) of cardiomyocytes. In this context, two separate questions concerning continuous model's suitability to describe cardiac conduction arise. The first one is whether the electric propagation phenomena in cardiac muscle—which is inherently discontinuous, with myocytes of 100 $\mu$m in length and 20 $\mu$m in diameter—can be described credibly by continuous cable equation (Eqs. 9 or 12). The second question—specifically pertaining to our model—is whether the very same cable equation, when discretized on a grid with internodal distance, say, $h = 0.05$ cm, is still adequate for accurately simulating cardiac propagation phenomena. Winfree [52] shows that the answer to these questions lies in the value of the directional diffusion coefficient in relation to spacing of cardiomyocytes (or model cells), and risetime of the action potential (which, in continuous bidomain theory, is assumed to be the same in all directions). As long as the directional diffusion coefficient "generously" exceeds (cell spacing)$^2$/(activation risetime) the continuous equation suffices for macroscopic purposes. Thus, along the fiber direction it is required that $D > (0.01\ \mathrm{cm})^2/0.0005\ \mathrm{s} = 0.2\ \mathrm{cm}^2/\mathrm{s}$, and in the transverse direction $D > (0.002\ \mathrm{cm})^2/0.0005\ \mathrm{s} = 0.008\ \mathrm{cm}^2/\mathrm{s}$. Although these inequalities are satisfied in our model (see Table 3), the required values are exceeded by a small margin and thus the answer to the second question must be only a qualified "yes." With model parameters such as those listed in Table 3, adequate precautions have to be taken (such as an incorporation of a "bulk factor" and carefully chosen stencils described in the Appendix).

## Bulk factor

By introducing the locally adjustable bulk factor defined in Eq. 19, we compensate for the macroscopic size of model cells by performing, in fact, time- and volume-integration of pertinent variables. The bulk factor takes into account that the activation wave-front's propagation across a given model cell is affected not only by anisotropic conductivities (since a directional velocity of propagation depends, under the assumption of uniform anisotropy and planar wave front, on the square root of directional conductivity) but possibly also by the directionally-dependent value of the membrane capacitance. Spach and colleagues observed a directionally-dependent wave front thickness resulting from structural discontinuities of cardiac muscle, and they showed that the observed differences are compatible with different values of specific membrane capacitance in different directions; normally, $\mathrm{C_m}$ is approximately 1 $\mu$F/cm$^2$ in the longitudinal direction, but it appears that it may be only 0.5 $\mu$F/cm$^2$ in the transverse direction [43].

Values of $\dot{V}_{max,\ell}$ and $\dot{V}_{max,t}$ given in Table 2 were measured in canine ventricular preparation [44]; values for human cardiac tissue are also available [43], but the latter measurements were obtained in an atrial preparation, with more pronounced anisotropic properties than in ventricles; values of $\dot{V}_{\mathrm{max}}$ obtained in isolated human ventricular myocytes [37] are much higher, because of the lack of loading effect caused by surrounding tissue.

The directionally-dependent bulk factor, determined during the simulation, is applied in "packaging" the transmembrane potential, $v_m$, and the transmembrane current, $I_m$. This "packaging" method has been thoroughly validated in the uniformly anisotropic slab. It follows from the one-dimensional cable equation [15] that the propagation velocity of an AP is proportional to the square root of conductivity. This relation is also valid for the two- and three-dimensional uniformly anisotropic media under the assumption of equal anisotropy ratio and for the planar activation wave front [29, 32, 51, 52, 53]. In the bidomain case, the ratio of propagation velocities can be approximated as a square root of the ratio

of harmonic mean conductivities defined in Eq. 2. Although the square-root relation for conduction velocities is generally not valid for general anisotropy cases [52], it can be used in the local basis to calculate directional bulk factor, provided assumptions of planar wave and uniform anisotropy are locally satisfied.

A more rigorous definition of the bulk factor would require evaluation of double (volume- and time-) integrals for the model cell's volume $h^3$ and the time required for the wave front of a given thickness (variable with direction of propagation) to transit through the model cell. However, even the simple approximation of the mean directional quantities based on the presently used estimate of the bulk factor produces noticeable improvements in the propagation algorithm, as judged by the close approximation of the ideal ellipsoid in the uniformly anisotropic medium, and by the stability of the algorithm in the medium with rotational anisotropy resembling transmural rotation of fibers in the ventricular wall.

### Previous studies of unequal anisotropy ratio

Previous studies of general anisotropy ratio [9, 14, 16, 38] used fine grids ($h \sim 100$ $\mu$m) in small blocks of excitable cells. Our hybrid approach is designed for whole-heart simulations and, therefore, has to accommodate larger grid sizes. For example, Roth [38] and Henriquez *et al.* [14] solved the elliptic equation, Eq. 4, using an iterative method, and then substituted the resulting $\phi_e$ into

$$\nabla \cdot G_i \nabla v_m = c_m \frac{\partial v_m}{\partial t} + i_{ion}(v_m) - \nabla \cdot G_i \nabla \phi_e \ .$$

Hooke *et al.* [16] showed that using this transformation, in terms of $v_m$ and $\phi_e$, allows one to solve the latter parabolic PDE using an explicit forward method. Di Cola *et al.* [9] solved the elliptic PDE by means of the semidiscrete Galerkin approximation, and the parabolic PDE using a linearization technique for the reaction term combined with the Crank-Nicholson time-stepping. The above mentioned studies used the Ebihara-Johnson model [10] to simulate the ionic current dynamics and action potentials.

The isochrones in our simulations with equal and harmonic-mean anisotropy ratios have elliptical shapes, and the estimated average propagation velocities are in very good agreement with the square-root relation derived by Muler and Markin [29, 51]. Moreover, the propagation velocities are in agreement with the velocities observed in isolated human hearts [8]. With the introduction of the bulk factor to take into account the large cell size, the algorithm could be adjusted to produce correct behavior for the model cells.

The ellipsoidal activation isochrones in Fig. 3 are identical regardless of the fiber orientation. Thus, the stencil for the electrotonic source computed from Eq. (17) is not directionally biased. Moreover, the activation isochrones follow the theoretical ellipsoidal shape closely. The observed propagation speed fits well with values obtained in other studies, indicating that the surface-to-volume ratio is correct. (The value of 2200 cm$^{-1}$ was estimated from the typical dimensions of cardiomyocytes observed on electron-micrographic images.)

### Limitations

The model is able to reproduce the foot of the AP as it would have been recorded by an electrode with diameter $h$. However, the large inter-cell distance introduces errors in the transmembrane current, as can be seen from the ratio of positive to negative area under the curve. Theoretically, and in microscopic recordings, the ratio should be close to one. The large spacing acts as a low-pass filter that widens the negative deflection and thus increases the negative area.

Spatial conduction is continuous after the modification of the propagation algorithm involving the bulk factor (Eq. 19). If the effect of bulking is neglegted, the activation appears to 'jump' between cells. When the cell goes into upstroke, it depolarizes very fast, and the neighboring cell detects the $v_m$ change that resembles a step function. With the bulk factor, the average membrane potential is used in the computation of electrotonic interaction. The effect of this is demonstrated in Fig. 6.

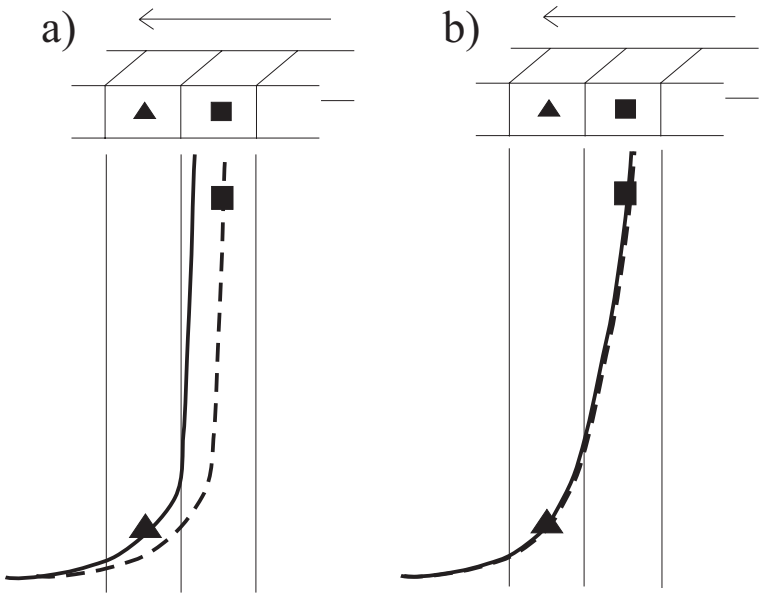


Figure 6: The application of the bulk constant makes the propagation of the AP spatially continuous. a) Without taking into account bulking, the AP upstroke due to ionic currents is too fast. The spatial APs derived from neighboring cells in subthreshold (triangle) and upstroke (square) state do not match. b) With bulking, the spatial AP is a well-defined continuous function that can be derived from the state of any active cell in the cell's neighborhood.

The stability of the simulations was improved significantly by computing the electrotonic source according to Eq. (17). After this modification, no unstable behavior could be observed.

The results also demonstrate that the same monodomain-type equation of the equal anisotropy ratio (Eq. 9) can be solved for unequal anisotropies (Eq. 12) at the same computational cost. There is still ongoing discussion regarding precisely what conductivities should be used.

### Conclusions

We have introduced modifications to the bidomain simulation algorithms of the previously developed hybrid model of the cardiac muscle that account for unequal conductivity ratios of conductivities in intracellular and interstitial domains, and for the relatively large size of the model cells compared to the thickness of the activation wave front. With these modifications, the simulated electrical propagation agrees with theoretical results, the propagation velocity is of the correct order, and the APs and transmembrane currents resemble measurements from real tissue. Our model allows simulations of propagated excitation in large and complex anatomical structures, such as the ventriclar myocardium, by assuming general anisotropy ratio and bypassing detailed modeling of transmembrane ionic currents during the cardiac AP.

## ACKNOWLEDGEMENTS

This study was supported by the Academy of Finland, Jenny and Antti Wihuri Foundation, Aarne Koskelo Foundation, the Pirkanmaa Cultural Foundation, the Heart & Stroke Foundation of Nova Scotia, the Canadian Institutes of Health Research (CIHR), and by a Collaborative Health Research Project grant from the Natural Sciences and Engineering Council of Canada (NSERC). The authors are also grateful to the experts at the Scientific Computing Ltd., for their help with the parallelized sparse-system solutions.

# References


[1] Berenfeld, O., and J. Jalife. Purkinje-muscle reentry as a mechanism of polymorphic ventricular arrhythmias in a 3-dimensional model of the ventricles. *Circ. Res.* 82:1063–1077, 1998.

[2] Burks, A.W., editor. *Essays on cellular automata*. University of Illinois Press, Urbana, IL, 1970.

[3] Cherry, E.M., H.S. Greenside, and C.S. Henriquez. A space-time adaptive method for simulating complex cardiac dynamics. *Phys. Rev. Lett.* 84:1343–1346, 2000.

[4] Clayton, R.H. Computational models of normal and abnormal action potential propagation in cardiac tissue: linking experimental and clinical cardiology. *Physiol. Meas.* 22:R15–R34, 2001.

[5] Clements, J.C., C.J. Clements, and B.M. Horáček. Wave-propagation dynamics in an anisotropic excitable medium. *Dynamics of Continuous, Discrete and Impulsive Systems Series* B: *Applications & Algorithms*. 10:469–480, 2003.

[6] Colli Franzone, P., L. Guerri, and B. Taccardi. Spread of excitation in a myocardial volume: Simulation studies in a model of anisotropic ventricular muscle activated by point stimulation. *J. Cardiovasc. Electrophysiol.* 4:144–160, 1993.

[7] Colli Franzone, P., L. Guerri, and S. Tentoni. Mathematical modelling of the excitation process in myocardial tissue: Influence of fiber rotation on wavefront propagation and potential field. *Math. Biosci.* 101:155–235, 1990.

[8] Durrer, D., R.Th. van Dam, G.E. Freud, M.J. Janse, F.L. Meijler, and R.C. Arzbaecher. Total excitation of the isolated human heart. *Circulation* 41:899–912, 1970.

[9] Di Cola, C., E. Macchi, and S. Sanfelici. Numerical simulation of activation in a bidomain model of cardiac muscle. *Med. & Biol. Eng. & Comp.* 34(Suppl. 1):87–88, 1996.

[10] Ebihara, L., and E.A. Johnson. Fast sodium current in cardiac muscle. *Biophys. J.* 32:779–790, 1980.

[11] Geselowitz, D.B., and W.T. Miller III. A bidomain model for anisotropic cardiac muscle. *Ann. Biomed. Eng.* 11:191–206, 1983.

[12] Gulrajani, R.M. Models of the electrical activity of the heart and the computer simulation of the electrocardiogram. *CRC Crit. Rev. Biomed. Eng.* 16:1–66, 1988.

[13] Henriquez, C.S. Simulating the electrical behavior of cardiac tissue using the bidomain model. *Crit. Rev. Biomed. Eng.* 21:1–77, 1993.

[14] Henriquez, C.S., A.L. Muzikant, and C.K. Smoak. Anisotropy, fiber curvature, and bath loading effects on activation in thin and thick cardiac tissue preparations: simulations in a three-dimensional bidomain model. *J. Cardiovasc. Electrophysiol.* 7:424–444, 1996.

[15] Hodgkin, A.L., and W.A.H. Rushton. The electrical constants of a crustacean nerve fibre. *Proc. R. Soc. Lond.* 133:444–479, 1946.

[16] Hooke, N., C.S. Henriquez, P. Lanzkron, and D. Rose. Linear algebraic transformations of the bidomain equations: implications for numerical methods. *Math. Biosci.* 120:127–145, 1994.

[17] Horáček, B.M., J. Nenonen, J.A. Edens, and L.J. Leon. A hybrid model of propagated excitation in the ventricular myocardium. In Ghista, D.N., editor, *Biomedical and Life Physics*, pages 181–190. Vieweg Verlag, Wiesbaden, 1996.

[18] Horáček, B.M., K. Simelius, R. Hren, and J. Nenonen. Challenges in modelling human heart's total excitation. In Katila, T., I.E. Magnin, P. Clarysse, J. Montagnat, and J. Nenonen, editors, *Lecture Notes in Computer Science 2230: Functional Imaging and Modeling of the Heart*, pages 39–46, Berlin, 2001. Springer-Verlag.

[19] Hren, R., J. Nenonen, and B.M. Horáček. Simulated epicardial potential maps during paced activation reflect myocardial fibrous structure. *Ann. Biomed. Eng.* 26:1022–35, 1998.

[20] Huiskamp, G.J. Simulation of depolarization in a membrane-equation-based model of the anisotropic ventricle. *IEEE Trans. Biomed. Eng.* BME-45:847–855, 1998.

[21] Jack, J.J.B., D. Noble, and R.W. Tsien. *Electric Current Flow in Excitable Cells*. Clarendon Press, Oxford, 1983.

[22] LeGrice, I.J., B.H. Smaill, L.Z. Chai, S.G. Edgar, J.B. Gavin, and P.J. Hunter. Laminar structure of the heart: Ventricular myocyte arrangement and connective tissue architecture in the dog. *Am. J. Physiol. Heart Circ. Physiol.* 269:H571–H582, 1995.

[23] Leon, L.J., and B.M. Horáček. Computer model of excitation and recovery in the anisotropic myocardium. I. Rectangular and cubic arrays of excitable elements. *J. Electrocardiol.* 24:1–15, 1991.

[24] Leon, L.J., and B.M. Horáček. Computer model of excitation and recovery in the anisotropic myocardium. II. Excitation in the simplified left ventricle. *J. Electrocardiol.* 24:17–31, 1991.

[25] Leon, L.J., and B.M. Horáček. Computer model of excitation and recovery in the anisotropic myocardium. III. Arrhythmogenic conditions in the simplified left ventricle. *J. Electrocardiol.* 24:33–41, 1991.

[26] Lewis, T.J., and M.R. Guevara. Chaotic dynamics in an ionic model of the propagated cardiac action potential. *J. Theor. Biol.* 146:407–432, 1990.

[27] Moe, G.K., W.C. Rheinboldt, and J.A. Abildskov. A computer model of fibrillation. *Am. Heart J.* 67:200–220, 1964.

[28] Muler, A.L., and V.S. Markin. Electrical properties of anisotropic nerve-muscle syncytia - I. Distribution of the electrotonic potential. *Biofizika* 22:307–312, 1977.

[29] Muler, A.L., and V.S. Markin. Electrical properties of anisotropic nerve-muscle syncytia. II. Spread of flat front of excitation. *Biofizika* 22:518–522, 1977.

[30] Nenonen, J., J.A. Edens, L.J. Leon, and B.M. Horáček. Computer model of propagated excitation in the anisotropic human heart. I. Implementation and algorithms. In A. Murray and R. Arzbaecher, editors, *Computers in Cardiology*, pages 545–548. IEEE Computer Society Press, Los Alamitos, CA, 1991.

[31] Nenonen, J., J.A. Edens, L.J. Leon, and B.M. Horáček. Computer model of propagated excitation in the anisotropic human heart. II. Simulation of extracardiac fields. In A. Murray and R. Arzbaecher, editors, *Computers in Cardiology*, pages 217–220. IEEE Computer Society Press, Los Alamitos, CA, 1991.

[32] Nicholson, P.W. Experimental models for current conduction in an anisotropic medium. *IEEE Trans. Biomed. Eng.* BME-14:55–56, 1967.

[33] Plonsey, R. *Bioelectric Phenomena*. McGraw-Hill, New York, 1969.

[34] Plonsey, R., and R.C. Barr. Current flow patterns in two-dimensional anisotropic bisyncytia with normal and extreme conductivities. *Biophys. J.* 45:557–571, 1984.

[35] Plonsey, R., and R.C. Barr. Mathematical modeling of electrical activity of the heart. *J. Electrocardiol.* 20:219–226, 1987.

[36] Pollard, A.E., M.J. Burgess, and K.W. Spitzer. Computer simulations of three-dimensional propagation in ventricular myocardium: Effects of intramural fiber rotation and inhomogeneous conductivity on epicardial activation. *Circ. Res.* 72:744–756, 1993.

[37] Priebe, L., and D.J. Beuckelmann. Simulation study of cellular electric properties in heart failure. *Circ. Res.* 82:1206–1223, 1998.

[38] Roth, B.J. Action potential propagation in a thick strand of cardiac muscle. *Circ. Res.* 68:162–173, 1991.

[39] Roth, B.J. A mathematical model of make and break electrical stimulation of cardiac tissue by a unipolar anode or cathode. *IEEE Trans. Biomed. Eng.* BME-42:1174–1184, 1995.

[40] Roth, B.J. Electrical conductivity values used with the bidomain model of cardiac tissue. *IEEE Trans. Biomed. Eng.* BME-44:326–328, 1997.

[41] Schmitt, O.H. Biological information processing using the concept of interpenetrating domains. In Leibovic KN, editor, *Information Processing in the Nervous System*, pages 325–331. Springer, New York, 1969.

[42] Spach, M.S. Transition from a continuous to discontinuous understanding of cardiac conduction. *Circ. Res.* 92:125–126, 2003.

[43] Spach, M.S., P.C. Dolber, J.F. Heidlage, J.M. Kootsey, and E.A. Johnson. Propagating depolarization in anisotropic human and canine cardiac muscle: apparent directional differences in membrane capacitance. A simplified model for selective directional effects of modifying the sodium conductance on $v_{max}$, $\tau_{foot}$, and the propagation safety factor. *Circ. Res.* 60:206–219, 1987.

[44] Spach, M.S., and J.F. Heidlage. A multidimensional model of cellular effects on the spread of electrotonic currents and on propagating action potentials. *Ann. Biomed. Eng.* 20:141–169, 1992.

[45] Spach, M.S., and R.C. Barr. Effects of cardiac microstructure on propagating electrical waveforms. *Circ. Res.* 86:e23–e28, 2000.

[46] Streeter Jr, D.D. Gross morphology and fiber geometry of the heart. In Berne RM, Sperelakis N, and Geiger SR, editors, *Handbook of physiology - Section 2: The cardiovascular system, Volume I: The heart*, pages 61–112. Am. Physiol. Soc., Bethesda, MD, 1979.

[47] Toffoli, T., and N. Margolus. *Cellular Automata Machines*. MIT Press, Cambridge, MA, 1987.

[48] Tung, L. *A Bidomain Model for Describing Ischemic Myocardial DC Potentials*. PhD thesis, Massachusetts Institute of Technology, Cambridge, MA, 1978.

[49] van der Vorst, H. Bi-CGSTAB: A fast and smoothly converging variant of Bi-CG for the solution of nonsymmetric linear systems. *SIAM J. Sci. Stat. Comput.* 13:631–634, 1992.

[50] Wiener, N., and A. Rosenblueth. The mathematical formulation of the problem of conduction of impulses in a network of connected excitable elements, spefically in cardiac muscle. *Arch. Inst. Cardiol. Mex.* 16:205–265, 1946.

[51] Winfree, A.T. Estimating the ventricular fibrillation threshold. In L. Glass, P. Hunter, and A. McCulloch, editors, *Theory of Heart: Biomechanics, Biophysics, and Nonlinear Dynamics of Cardiac Function*, pages 477–528. Springer, New York, 1991.

[52] Winfree, A.T. Heart muscle as an excitable medium: the roles of wavefront curvature and anisotropy. *Int J. Bifurc. Chaos* 7:487–526, 1997.

[53] Winfree, A.T. A spatial scale factor for electrophysiological models of myocardium. *Prog. Biophys. Mol. Biol.* 69:185–203, 1998.

[54] Winslow, R.L., D.F. Scollan, A. Holmes, C.K. Yung, J. Zhang, and M.S. Jafri. Electrophysiological modelling of cardiac ventricular function: from cell to organ. *Annu. Rev. Biomed. Eng.* 2:119–155, 2000.

# APPENDIX

## Computation of partial derivatives

Partial derivatives are estimated as differentials computed in a neighborhood of the center cell. Estimation of higher-order partial derivatives for a function is usually done with a Taylor expansion in the neighborhood of a central point. (We chose to use 19 cells, including the central cell, from the neighborhood of $3 \times 3$ cells.) This method regularly yields estimates that are $\mathcal{O}(h^2)$, but $\mathcal{O}(h^4)$ estimates are also easy to construct. In our case, stability of the estimates in iterative computations is more important than high accuracy, since the period when the cells are interacting is rather short in terms of the number of timesteps. For this reason, the estimation error does not accumulate, but a stencil must be carefully chosen to avoid erratic behavior of the propagation algorithm. The stencils for different derivatives are described below.

**The cross derivatives** in Eq. 15 would be easy to evaluate by a square stencil, where the first and third quadrant receive a weight of 1.0 and the second and fourth a weight of $-1.0$. However, we found such simple estimation of cross derivatives inadequate, and thus we considered instead two other candidates for stencils in an 18-neighbor environment. The first one, a "corner stencil," used the corners of a $3\times3$ square and consequently had a spacing $2h$. This stencil is a sum of four unit stencils; when these four stencils are added, all the cells in the middle cancel out. Because we observed instability in the "corner stencil," we finally chose to use a diagonally asymmetric stencil, which is constructed by including only two of the smaller stencils used in the "corner stencil." This way, we can use 7 of the 9 points available for the computation, and the stencil has no gaps. Most importantly, the center cell is included in this stencil with a weight of 2. To prevent overestimation of the cross derivative, the orientation of the stencil is always chosen so that we get a smaller result of the two possible ones. In other words, the stencil is aligned to the wave front; this alignment is done as a part of the propagation algorithm.

**The second derivatives** in Eq. 15 are computed by using a longitudinal stencil of (1,-2,1) at the center cell. For example, $f_{xx}(x, y, z) = f(x - h, y, z) - 2f(x, y, z) + f(x + h, y, z)$. Averaging of second derivatives from neigbouring cells would introduce excessive smoothing.

**The Laplacian** in Eq. 15 ($f_{xx} + f_{yy} + f_{zz}$) can be estimated by any totally symmetric and zero-sum stencil, where the center cell has a negative weight. The most accurate coefficients for computing the estimate can be calculated by writing the analytical expression for Taylor series expansion up to the sixth term, and requiring that the $\mathcal{O}(h^2)$ and $\mathcal{O}(h^3)$ terms cancel. The resulting coefficients weight the stencil heavily in the direction of the coordinate axes. On the other hand, a perfectly even weighting would result in a very stable estimate for the simulations. We chose a method that weights the 6 closest neighbors by 4.0 and the other 12 by 1.0, which yields a central weight of $-36.0$.

**The gradient** in Eq. (16) is computed simply as the difference in $\phi$ divided by the distance between the cells: $\nabla f = \sum_{k=1}^{26}(f_k - f_0)/d_k$, where $f_0$ is the value at the center and $d$ is the distance between the elements (i.e., $h$, $h\sqrt{2}$, or $h\sqrt{3}$). The weight on the diagonal neighbors and "corners" is thus reduced, correspondingly, to $1/\sqrt{2}$ and $1/\sqrt{3}$, which improves stability.

**ISBN 951-22-7026-9**
**ISSN 1459-7268**